Secondary Gas Injection in a Conical Rocket Nozzle[1]

R. E. Walker,[2] A. R. Stone,[3] and M. Shandor[4]
Applied Physics Laboratory, Johns Hopkins University, Silver Spring, Md.

Data are presented on side forces generated by secondary gas injection in a 15° conical rocket exhaust nozzle. The side force was measured directly with a force transducer and the data examined in terms of an amplification factor I_s/I_s^*, where I_s is the measured effective specific impulse of injectant, and I_s^* is the specific impulse of injectant for sonic flow into a vacuum. Injection was normal to the axis of the nozzle through a single circular orifice at a fixed point in the diverging portion of the nozzle. A variety of ambient temperature gaseous injectants (H_2, He, He + Ar, N_2, CO_2, and Ar) and orifice diameters were carefully studied. Injectant flow rate was varied for each configuration. The main propellant was hot gas (catalytically decomposed 90% H_2O_2), and motor conditions were held essentially constant.

Nomenclature

A_j = jet orifice area
A_t = nozzle throat area
A_1 = nozzle area at point of injection
C_D = discharge coefficient of orifice assuming sonic flow
d_j = orifice diameter
F_N = side force due to secondary injection
F = axial thrust of motor
g = gravitational constant
I_s = $F_N/\dot{W}_j$, effective specific impulse of injectant
I_s^* = $\frac{1}{g}\left[\frac{2(1+\gamma_j)RT_{0j}}{\gamma_j \mathfrak{M}_j}\right]^{1/2}$, specific impulse of vacuum-exhausted sonic jet of injectant (see Table 2 for values)
M_1 = Mach number of nozzle flow at point of injection
$\mathfrak{M}$ = molecular weight of propellant gases
$\mathfrak{M}_j$ = molecular weight of injectant
P_1 = static pressure of nozzle flow at point of injection
P_2 = static pressure behind induced oblique shock wave
P_0 = stagnation pressure of propellant gases
P_{0j} = stagnation pressure of injectant
P_j = static pressure of injectant at orifice
R = universal gas constant
T_0 = stagnation temperature of propellant
T_{0j} = stagnation temperature of injectant
$\dot{W}_j$ = mass flow rate of injectant
$\dot{W}$ = mass flow rate of propellant
γ = specific heat ratio of propellant
γ_j = specific heat ratio of injectant

Recent advances in solid rocket propellant technology, resulting in higher flame temperatures and multiphase flow, place a premium on thrust vector control methods that minimize exposure of moving parts to propellant exhaust products. Fluid injection is one method receiving considerable attention. This technique uses asymmetric wall forces caused by lateral injection of a fluid (gas or liquid) into the divergent portion of the rocket exhaust nozzle. In addition to the usual jet reaction, local high pressures associated with an induced shock wave "amplify" the jet reaction. The first experiments on secondary injection were reported by Hausmann (1),[5] and they demonstrated that the shock-induced reaction associated with an air jet directed into supersonic air (both gases at ambient temperature) could be as large as the jet reaction. The nature of this shock-induced reaction and the way in which it depends upon the mainstream and injectant properties have since been the subject of considerable study, mostly experimental. Several experiments have been reported for jet-interference phenomena on simple aerodynamic surfaces (2–6), on the external surfaces of simple missile configurations (7–9), and on the internal surfaces of rocket nozzles, i.e., secondary injection (10–16). Most of these reports deal with ambient temperature air-air interaction. Because of the complexity of the problem, analytical descriptions have been quite limited. For gas injection, two qualitatively correct basic descriptions have been useful (8, 17–19), but refinements are desirable.

This paper presents the results of experiments performed at this laboratory on secondary gas injection into hot supersonic propellant flow in a small rocket motor. Data on the effects of injectant gas properties and injectant orifice size have been obtained; motor operating conditions, nozzle geometry, and injectant location have been kept fixed. Future experiments involving temperature effects, nozzle geometry, point of injection, and mainstream properties are planned.

Description of Experimental Apparatus and Testing Procedure

Apparatus

The data presented in this report were obtained with a small research rocket motor and nozzle, sketched in Fig. 1. The working fluid was provided by catalytic decomposition of 90% hydrogen peroxide liquid[6] at a nominal motor chamber pressure of 400 psia. The products of decomposition were 29.2% mole fraction of oxygen and 70.8% mole fraction of water vapor, with a specific heat ratio of 1.266 (20). Average propellant exhaust temperature, measured with an uncalibrated iron-constantan thermocouple, was 1845°R, with a maximum spread of 1830° to 1865°R. This temperature is slightly higher than the theoretical adiabatic decomposition temperature, 1825°R (20).

Some motor, nozzle, and injectant properties are listed in Table 1. Attempts to measure the liquid propellant flow rate $\dot{W}$ were unsuccessful. It was therefore necessary to rely upon motor chamber pressure P_0 and temperature T_0 (=1845° R), geometrical area of the nozzle throat A_t (0.196 in.^{2}), and isentropic flow relations to compute propellant flow rate, theoretically, $\dot{W} = 0.00208\ P_0$, where $\dot{W}$ is in pounds per second and P_0 is in pounds per square inch absolute; P_0 = 390 to 420 psia for these tests.

The average thrust coefficient C_F for motor chamber pressure of about 400 psia has been found experimentally to be 1.42, which is somewhat below the theoretical value of 1.46 (based upon conical isentropic nozzle flow and area ratio for P_0 = 400 psia and an atmospheric pressure of 14.7 psia). Axial thrust F for these experiments can be computed closely from $F = C_F A_t P_0 \approx 0.278\ P_0$, with F in pounds and P_0 in pounds per square inch absolute.

Received by ARS May 31, 1962; revision received September 12, 1962.
[1] This work was sponsored by the Special Projects Office, Bureau of Naval Weapons.
[2] Project Supervisor, Jet Controls. Member AIAA.
[3] Senior Engineer. Member AIAA.
[4] Associate Physicist. Member AIAA.
[5] Numbers in parentheses indicate References at end of paper.

[6] Supplied by Becco Chemical Division, Food Machinery and Chemical Corporation.

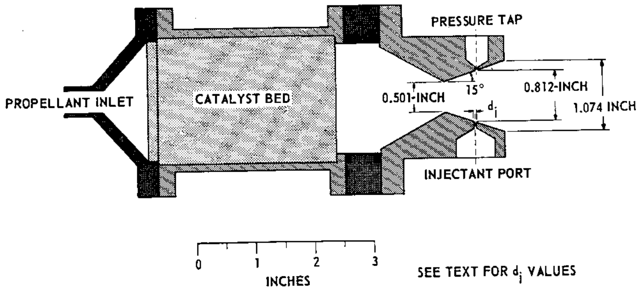

Fig. 1 Research rocket motor used in secondary gas injection experiments

Injectant gases were obtained from standard compressed gas containers.[7] A maximum injectant pressure of about 500 psia was used for carbon dioxide and about 1000 psia for the other gases; injectant gas temperature was ambient, nominally 70°F. The injectant gas flow rate was metered through a standard ASME sharp-edged orifice flowmeter calibrated with CO_2 by timed discharge into a calibrated volume. Molecular weight and compressibility corrections were made in the usual manner when the other injectant gases were used. Evaluation of the discharge coefficient of injectant orifice in the nozzle wall was made by using a combination of this metered flow rate $\dot{W}_j$, measured jet total pressure P_{0j}, total temperature T_{0j}, geometric orifice area A_j $(=\pi d_j^2/4)$, and isentropic flow relations. This calculation provided a compatibility check for several measured parameters.

Fig. 2 shows the general setup of the apparatus. The motor is mounted on the periphery of and in line with the axis of a drum, the axle of which is mounted in antifriction bearings that permit simultaneous rotation and axial motion. The drum floats in water to reduce bearing load. Force transducers measure axial motor thrust and turning moment developed by secondary injection or by motor trim misalignment. Propellant and injectant go to the nozzle through relatively long rigid lines, which, by test, were found to introduce fixed spring constants superimposed on the elastic constants of the force transducers. Transducer calibrations are obtained after or during each day of operation with the transducers in place.

Most pressure measurements were made with a variety of electrical pressure transducers that were calibrated periodically with Bourdon element test gages. The gages in turn were calibrated against a standard dead weight tester. Where possible, all transducers were excited from a common monitored supply voltage, and observed variations in excitation voltage were included in the data analysis. Temperature measurements were made with uncalibrated iron-constantan thermocouples. Appropriately attenuated transducer and thermocouple outputs were recorded on four 0 to 1 mv, 10-in. Westronics strip-chart recorders either continuously or through a dual six-point data sampler that permits more than one bit of information per recorder channel.

Testing Procedure

Because of possible transients, the following operating sequence was adopted:

1) One complete data sampling sequence ($\approx$12 sec), without propellant or injectant flow, to establish transducer and recorder zeros. No special effort was made to pre-adjust transducer outputs to zero.

2) Propellant-on/injectant-off sequence to determine thrust misalignment (motor trim).

3) Propellant-on/injectant-on to measure secondary injection effects.

[7] Carbon dioxide for these experiments was supplied by Pure Carbonic Company. All other gases were supplied by Southern Oxygen Company.

Table 1 Properties of research rocket motor, nozzle, and injectants used in secondary gas injection experiments

Motor	
Propellant	90% H_2O_2
Exhaust gas composition	0.708 mole fraction H_2O; 0.292 mole fraction O_2
Thrust coefficient C_F	1.42
Pressure P_0	$\approx$400 psi
Propellant flow rate $\dot{W}$	$\approx$0.84 lb/sec
Exhaust gas total temperature T_0	1845°R
Specific heat ratio γ	1.266
Ambient pressure	atmospheric
Injectant	
Gas	CO_2, N_2, He, He + Ar, Ar, and H_2
Injectant pressure P_{0j}	40 to 1000 psi
Injectant total temperature T_{0j}	$\approx$70°F
Injectant port diameter d_j	0.0625, 0.089, 0.125, 0.180 in.
Nozzle (conical, sharp-edged throat)	
Divergent half angle α	15°
Throat diameter d_t	0.501 in.
Exit diameter d_3	1.074 in.
Nozzle diameter at injectant port d_1	0.812 in.
Mach number at injection plane M_1	2.34
Exit Mach number M_3	2.83

4) Repetition of step 2 to determine trim change, if any.

5) Repetition of step 1 to determine transducer zero shift, if any.

This procedure permits all bits of information to be extrapolated and evaluated at a common time.

Experimental Results

Data were obtained on the separate effects of 1) injectant orifice size, and 2) injectant gas type. Only injection normal to the nozzle axis was examined. The motor chamber pressure was kept at the experimental maximum value of about 400 psia. The propellant gases had a stagnation temperature close to 1845°R.

The injectant port, a single circular orifice, was located at the point in the conical expansion nozzle where the Mach number M_1 was 2.34. This Mach number was determined both by the experimentally measured pressure ratio $P_1/P_0 = 0.0730$ and by the geometrical area ratio $A_1/A_t = 2.597$. The static pressure of the undisturbed supersonic flow at the injection point was nominally 30 psia. The exit Mach number of the nozzle M_3 was computed from the geometrical area ratio A_3/A_t to be 2.83. The exhaust gases were overexpanded slightly at the nozzle exit, $P_3 = 12.8$ psia. No attempt was

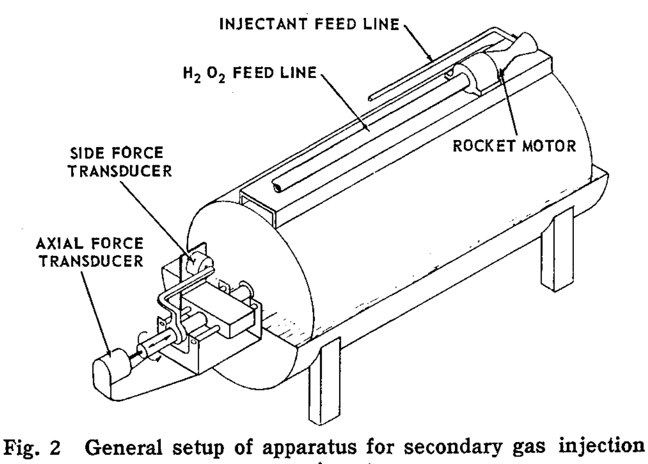

Fig. 2 General setup of apparatus for secondary gas injection experiments

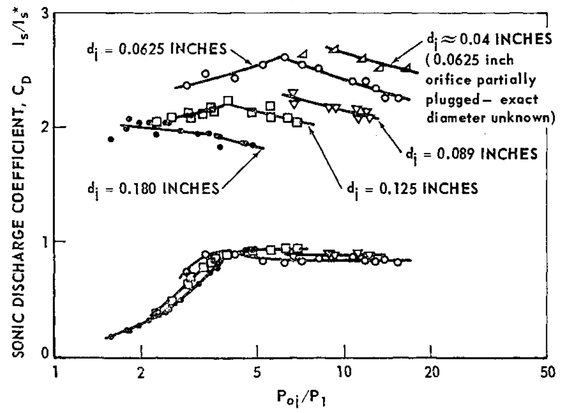

Fig. 3 Effect of orifice area on secondary gas injection (CO_2 injectant at 70°F)

made to reduce P_0 in order to examine secondary-injection-induced separation effects.

In the study of the effects of orifice size, carbon dioxide at ambient temperature (nominally 70°F) was selected as the injectant, and the orifice diameter d_j was varied from 0.0625 to 0.180 in. Changes in the orifice size were accomplished by simply "drilling out" the just-tested orifice. This practice gives a kind of thick, square-edged orifice whose discharge coefficient can be expected to depend strongly on Reynolds number and pressure ratio across the orifice. The variation in this pressure ratio P_{0j}/P_1, brought about by varying the jet mass flow, was sufficient to give both subsonic and sonic flow through the orifice ($1.4 < P_{0j}/P_1 < 12$). In retrospect, carbon dioxide was a poor choice for a working gas since, at the pressures and temperatures involved, significant compressibility effects were encountered. (For example, at 500 psia and 70°F, the compressibility factor for carbon dioxide is 0.79 and represents a considerable and measurable departure from ideal gas behavior.) Compressibility effects were taken into account when evaluating the orifice discharge coefficient by using a linearized treatment given by Eggers (21) for a calorically perfect but thermally imperfect gas. Separate experiments were performed to establish the validity of using this linearized analysis. No other compressibility effect corrections were made to the data.

A summary plot of the data pertaining to effect of orifice size is provided in Fig. 3, where the normalized specific impulse I_s/I_s^* and sonic discharge coefficient C_D are plotted as a function of jet pressure ratio P_{0j}/P_1.[8]

The effective specific impulse I_s is obtained by dividing the force normal to the motor axis F_N by the measured jet mass flow $\dot{W}_j$; I_s^* is the specific impulse of a sonic jet of the injectant exhausting into a vacuum. Values of I_s^* for various gases are listed in Table 2; I_s/I_s^*, therefore, represents an amplification factor for secondary injection.[9]

The sonic discharge coefficient C_D is obtained by dividing the measured jet mass flow by a theoretical value based upon sonic isentropic flow, the geometrical area of the orifice, and measured values of P_{0j} and T_{0j}. The breaking away of C_D from a constant value near unity is interpreted to be a transition from sonic to subsonic injection. As seen in Fig. 3, the knee of the C_D curve occurs at a value of P_{0j}/P_1 larger than the critical pressure ratio for jet flow without supersonic cross-flow interference. This results from higher effective back pressures brought about by the induced shock wave. Note also that the I_s/I_s^* curve tends to peak at or near this transition point and does not exhibit a monotonically increasing behavior for a decreasing P_{0j}/P_1, as might be inferred from theory (8,17).

Finally, the strong dependence of secondary injection effectiveness upon orifice size should be recognized. The variation in d_j examined here exceeds that studied by others, and the consequence of varying d_j has not been pointed out before.

Table 2 Some properties of the injectants used in secondary gas injection studies

Gas	$\mathfrak{M}_j$	γ_j	I_s^* (sec) at 70°F
CO_2	44.01	1.30	45.3
N_2	28.02	1.40	54.9
Ar	39.91	1.67	44.7
0.8 He + 0.2 Ar[a]	11.18	1.67	84.4
He	4.00	1.67	141.2
H_2	2.02	1.40	204.8

[a] Mole fractions.

Several gases have been used to investigate the effects of injectant molecular weight $\mathfrak{M}_j$ and specific heat ratio γ_j; the gases used are listed in Table 2. All of these injectants are inert, with the exception of H_2, which, in principle, could react with the hot O_2-H_2O propellant exhaust products. As will be seen later, there was no evidence of combustion. The observed failure to ignite may be attributed to the low exhaust temperature, which presumably is inadequate to support supersonic combustion (22). A summary plot is given in Fig. 4 (see Ref. 24). Ambient temperature injection through a 0.0625-in.-diam orifice has been used throughout. The extreme spread in experimental I_s (from 90 sec for Ar to 480 sec for H_2, about a factor of 5) is largely removed by using the parameter I_s/I_s^*. With I_s/I_s^*, the spread is about ±15%. This spread, the authors feel, is still outside experimental error. Characteristics associated with subsonic and sonic injection are similar to the data presented in Fig. 3.

A series of experiments was undertaken to determine the gain in axial motor thrust as a result of secondary injection. Ambient temperature injection of CO_2 through a 0.180-in.-diam orifice was used. The axial thrust change $\Delta F/(F_N \tan\alpha)$ was computed and found to be 1.30 ± 0.09, which was independent of $\dot{W}_j$ within the accuracy of the experiment. Since the pressure rise associated with secondary injection is distributed about the circumference of the nozzle, and since F_N is the integrated force component in the plane containing the orifice and nozzle centerlines, a value of $\Delta F/(F_N \tan\alpha)$ larger than unity (flat plate value) is to be expected.

Discussion of the Data

The data presented in Fig. 3 on the effect of injectant orifice diameter were taken in order to examine the theoretical postulate that the effectiveness of secondary injection should increase as the P_{0j}/P_1 ratio is decreased (8,17). This diverging characteristic has been observed in a number of experiments reported by others, but the low pressure ratio extremes have not been examined critically. The sonic injection data presented in Fig. 3 show the characteristic decline that also has been observed by others in secondary injection performance for increasing P_{0j}/P_1 ratios.

[8] A detailed listing of the data is given in Ref. 24.

[9] For these experiments, I_s/I_s^* seems preferable to other forms of the amplification factor. Usually $(F_N/\dot{W}_j) \div (F/\dot{W})$ is used, but this is strongly dependent upon $\mathfrak{M}_j$ and γ_j, whereas I_s/I_s^* is not. Since $\dot{W}$ and $F/\dot{W}$ were almost constant for these experiments ($\dot{W} \approx 0.83$ lb/sec, $F/\dot{W} \approx 133$ sec), inclusion of $F/\dot{W}$ in a correlation could be misleading. One can easily convert these data to this form; I_s^* values are given in Table 2, and $F/\dot{W} \approx 133$ sec. The original report (24) should be consulted for a detailed listing of the data. One must bear in mind that $F/\dot{W}$ depends upon motor conditions (P_0, T_0, $\mathfrak{M}$, and γ), nozzle contour, and expansion ratio.
Sometimes $F_N/[P_jA_j(1 + \gamma_jM_j^2) - P_1A_j]$ is used as an amplification factor. This form is difficult to use for subsonic injection since P_j and M_j cannot be accurately computed. Therefore, its use has been avoided. If $M_j = 1$, $F_N/[P_jA_j(1 + \gamma_jM_j^2) - P_1A_j] = I_s/(I_s^* - P_1A_j/\dot{W}_j) > I_s/I_s^*$. One form seems about as good as the other, since neither has any established uniqueness.

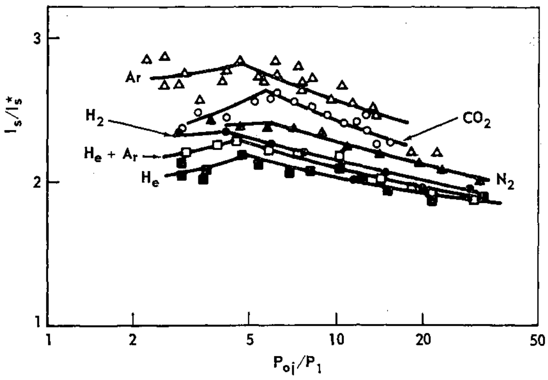

Fig. 4 Correlation of secondary injection data for various injectant gases ($d_j = 0.0625$ in., T_{0j} = 70°F)

However, this trend does not prevail for subsonic injection; it has been observed that, as the jet becomes subsonic (as indicated by the knee in the discharge coefficient curve), performance tends to *decrease* slightly with decreasing P_{0j}/P_1. The most efficient performance is achieved at or near the transition from sonic to subsonic injection. This behavior is not unique to this experiment (15). It is worthwhile to point out that this transition pressure ratio $(P_{0j}/P_1)_{tr}$ is compatible with an effective jet back pressure that will give combined "just-choked" jet flow and turbulent boundary layer separation of the mainstream ahead of the port. The pressure rise to give turbulent boundary layer separation for $M_1 \approx 2.4$ air is approximately $(P_2/P_1)_{sep} \approx 2.2$ (23). If one assumes that the static pressure at the jet orifice P_j is approximately equal to the pressure in the separated region P_2, then

$$(P_{0j}/P_1)_{tr} \approx (P_0/P)^*(P_2/P_1)_{sep} \approx (2.0)(2.2) = 4.4$$

which is in reasonable agreement with Fig. 3.

Additional information on the pressure rise associated with the induced shock wave can be obtained from the subsonic injection data in the following manner. If one assumes one-dimensional isentropic flow for the jet gases and a discharge coefficient equal to its asymptotic value at large P_{0j}/P_1, the static pressure at the jet orifice P_j can be evaluated from the measured values of $\dot{W}_j$, P_{0j}, T_{0j}, and A_j. In addition, assume that $P_j \approx P_2$. The results of such calculations for the subsonic CO_2 injection data appear in Fig. 5. For P_{0j}/P_1 less than about 3, the pressure rise P_2/P_1 increases almost linearly with P_{0j}/P_1 (increasing jet flux). For P_{0j}/P_1 greater than about 3, P_2/P_1 tends to level off at approximately a value required to give turbulent boundary layer separation. This would suggest that the induced oblique shock wave is probably attached initially to the leading edge of the orifice, and its strength increases with increase in jet flux until it reaches a limiting pressure rise sufficient to give separation. The shock then detaches from the orifice lip and moves upstream with increasing P_{0j}/P_1. This interpretation is compatible with the theoretical model given by Vinson et al. (8).

The weak jet model of Vinson et al. (8) does not present a qualitatively correct interpretation of the subsonic injection data for which it should be most applicable; i.e., it does not predict a decreasing I_s/I_s^* for decreasing P_{0j}/P_1. This characteristic has not been demonstrated for any known theoretical description.

In addition, the strong influence that d_j has upon the effectiveness of secondary gas injection, as shown by the data in Fig. 3, has not been established in the reports of other experiments and was not anticipated. Theory has not been developed to the point of including three-dimensional effects and is of no help in interpreting these data.

It is quite interesting, however, to replot the data of Fig. 3 as I_s/I_s^* vs $\dot{W}_j/\dot{W}$, which is essentially the form frequently used by others to report secondary injection data. Fig. 6 is

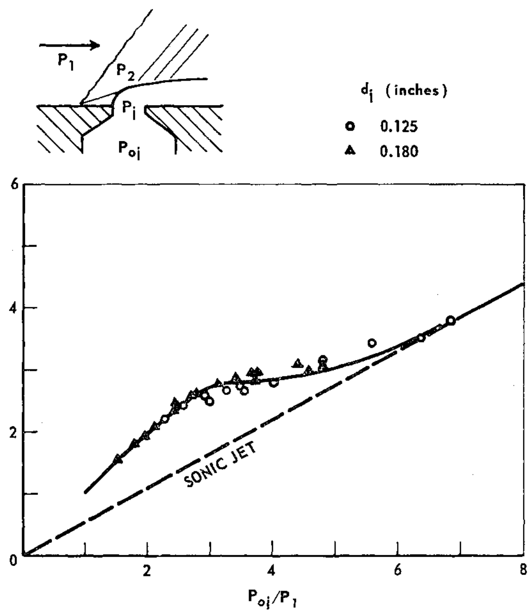

Fig. 5 Approximate pressure rise due to induced shock wave (subsonic CO_2 injection data)

such a graph and shows that all *sonic* CO_2 injection data correlate rather well. (The subsonic injection data do not correlate on this plot.) The reason for the correlation is not clear, since the independent variable $\dot{W}_j/\dot{W}$ suggests a kind of one-dimensional flow neither physically plausible nor consistent with restriction of the induced oblique-shock pressure rise (approximately) to within the Mach cone emanating from the wall-jet perturbation. It must be concluded that the effect of d_j on secondary gas injection is not well understood, and a more comprehensive analytical model would be welcomed.

From Fig. 4, it appears that variations in injectant molecular weight and specific heat ratio are largely accounted for by using the parameter I_s/I_s^*. However, second-order molecular weight effects are apparent, since gases with the same specific heat ratio but different molecular weight (for example, He, He + Ar, and Ar) give different I_s/I_s^* vs P_{0j}/P_1 plots. There is also some indication that specific heat ratio effects are not

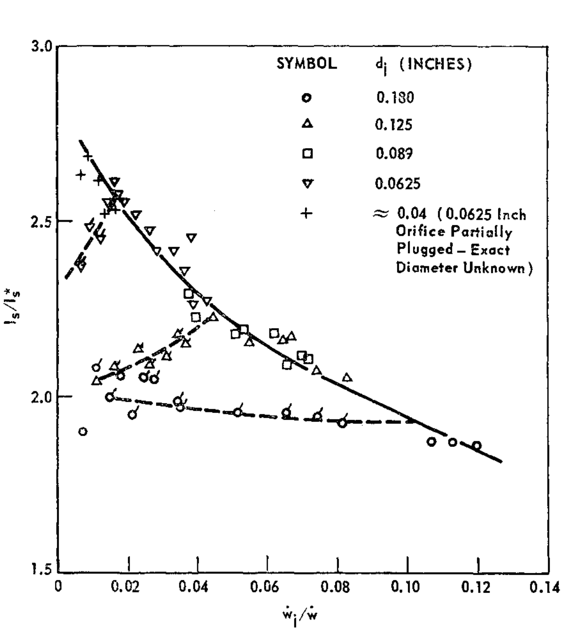

Fig. 6 Correlation of sonic secondary injection data [CO_2 injectant at 70°F; all subsonic injection data ($P_{0j}/P_1 \leq 4.0$) are flagged]

completely removed with I_s/I_s^*. For these data, P_{0j}/P_1 seems an appropriate independent variable; mass flow ratio would not be appropriate as in the data of Fig. 6.

Because the H_2 injection data appear to correlate well with other inert gas injection data, it has been concluded that no combustion takes place between the H_2 and the hot H_2O-O_2 exhaust gases. This conclusion is consistent with the research of Chinitz and Gross (22), who reported that combustion between H_2 and heated supersonic air does not occur below a critical stagnation air temperature of about 2000°F. By inference, the relative effect of changing injectant total temperature also can be predicted, but additional data on this parameter would be desirable.

Additional experiments designed to measure the effects of other parameters (such as T_{0j}, T_0, M_1, P_1, and nozzle geometry) are desirable in order to establish appropriate theoretical avenues. Some of these experiments are presently in progress at this laboratory.

Summary

This paper is the first in a series dealing with an experimental study of thrust vector control using gaseous secondary injection. For this study, the main propellant was a hot gas (catalytically decomposed H_2O_2); a variety of gases (CO_2, N_2, Ar, 0.8 He + 0.2 Ar, He, and H_2) at ambient temperature was used as the injectant. A conical convergent-conical divergent exhaust nozzle was used, with injection normal to the nozzle axis at a fixed point in the divergent portion of the nozzle.

A variety of circular orifice diameters (0.180, 0.125, 0.089, 0.0625, and 0.04 in.) was examined. The side force developed by secondary injection was measured directly with a force transducer; the data are reported as specific impulse ratio or "amplification factor," obtained by dividing the measured effective specific impulse of the injectant by the specific impulse of the injectant for sonic flow into a vacuum.

As the orifice diameter was varied (with CO_2 injectant), low-pressure injection was examined critically. The results showed that for a particular orifice size the amplification factor has a maximum at or near the transition from sonic to subsonic injection. Performance does not increase indefinitely for decreasing pressure ratio across the orifice, as might be construed from simple linear supersonic flow theory. Significant effects of orifice size on the specific impulse ratio were observed. For a fixed pressure ratio across the orifice, performance increases with decreasing orifice size.

Subsonic injection data aided in estimating the strength of the shock wave induced in the supersonic flow. These data have shown indirectly that shock wave strength increases to a limiting value close to that required for shock wave-turbulent boundary layer separation.

Performance of several inert gas injectants with differing molecular weights and specific heat ratios correlated well with the amplification factor I_s/I_s^*. One potentially reactive injectant (H_2) was used; its data correlated well with the inert gas data. This suggests that essentially no reaction occurred in the nozzle between the injectant and propellant.

Additional experiments designed to measure the effects of other parameters (such as injectant temperature, motor temperature and pressure, and injection and nozzle geometry) are desirable to establish appropriate theoretical avenues. Some of these experiments are presently in progress at this laboratory.

Acknowledgments

The authors would like to express their appreciation to E. Schmidt and J. Loveless of the APL/JHU High Temperature Laboratory for their assistance in the laboratory, to I. Soslow for preparation of drawings and figures, and to R. H. Cramer for his continuing interest during the course of this investigation.

References

1 Hausmann, G. F., "Thrust axis control of supersonic nozzles by airjet shock interference," United Aircraft Corp. Rept. R-63143-24 (May 2, 1952).

2 Amick, J. L. and Hayes, P. B., "Interaction effects of side jets issuing from flat plates and cylinders alined with a supersonic stream," Wright Air Dev. Div. TR 60-329 (May 1960).

3 Liepman, H. P., "On the use of side-jets as control devices," ARS J. **29**, 453–454 (1959).

4 Janos, J. J., "Loads induced on a flat-plate wing by an air jet exhausting perpendicularly through the wing and normal to a free-stream flow of Mach number 2.0," NASA TN D-649 (March 1961).

5 Cubbison, R. W., Anderson, B. H., and Ward, J. J., "Surface pressure distributions with a sonic jet normal to adjacent flat surfaces at Mach 2.92 to 6.4," NASA TN D-580 (February 1961).

6 Romeo, D. J. and Sterrett, J. R., "Aerodynamic interaction effects ahead of a sonic jet exhausting perpendicularly from a flat plate into a Mach number 6 free stream," NASA TN D-743 (April 1961).

7 Amick, J. L., Bond, C. E., and Liepman, H. P., "An experimental investigation of the forces and flow field produced by a jet exhausting laterally from a cone-cylinder in a Mach 2.84 stream," Univ. Mich., Dept. Aeronaut. Eng. WTM-255 (November 1955).

8 Vinson, P. W., Amick, J. L., and Liepman, H. P., "Interaction effects produced by jet exhausting laterally near base of ogive-cylinder model in supersonic main stream," NASA Memo. 12-5-58W (February 1959).

9 Carvalho, C. F. and Hays, P. B., "Jet interference experiments employing body-alone and body-fin in configuration at supersonic speeds," Univ. Mich. CM-979 (December 1960).

10 Lingen, A., "Jet-induced thrust-vector control applied to nozzles having large expansion ratios," United Aircraft Corp. Rept. R-0937-33 (March 1957).

11 Parker, G. H. and Edwards, S., "A theoretical and experimental investigation of a method of thrust vector control for solid rocket motors," Naval Ordnance Rept. NAVORD 5904, Vol. II (December 1959).

12 McAulay, J. E. and Pavli, A. J., "A cold flow investigation of jet-induced thrust-vector control," NASA Tech. Memo. X-416 (December 1960).

13 Rodriguez, C. J., "An experimental investigation of jet-induced thrust vector control methods," Bull. 17th Meeting, JANAF-ARPA-NASA Solid Propellant Group, Vol. III (May 1961).

14 Drewry, D. G., Hnatiuk, B. T., Kallmeyer, T. E., Harmoning, H. D., Hanley, D. P., and Hug, D. P., "Propellant gas injection for thrust vector control of solid propellant rockets," Bull. 17th Meeting, JANAF-ARPA-NASA Solid Propellant Group, Vol. II (May 1961).

15 Slates, R. O., Geres, R. J., Benham, C. B., and Johanson, D. F., "Research on secondary gas injection for thrust vector control applications," U. S. Naval Ordnance Test Station TP2856 (April 1962).

16 Chamay, A. J. and Sederquist, R. A., "An experimental investigation of shock vector control with gaseous secondary injection," ARS Preprint 2216-61 (October 1961).

17 Ferrari, C., "Interference between a jet issuing laterally from a body and the enveloping supersonic stream," Johns Hopkins Univ., Appl. Phys. Lab., Bumblebee Rept. 286 (April 1959).

18 Wu, J. M., Chapkis, R. L., and Mager, A., "An approximate analysis of thrust vector control by fluid injection," ARS J. **31**, 1677–1685 (1961).

19 Morgan, E. J., "An analysis of fluid injection into rocket nozzles," ARS Preprint 2335-62 (January 1962).

20 "Hydrogen peroxide physical properties data book," Becco Research and Dev. Dept., Bull. 67 (1955).

21 Eggers, A. J., Jr., "One-dimensional flows of an imperfect diatomic gas," NACA Rept. 959 (1950).

22 Chinitz, W. and Gross, R. A., "Exploratory studies of combustion in supersonic flow," Fairchild Engine and Airplane Corp., Project Squid, Office Naval Research Contract NR 1858 (25) NR-098-038 (June 1959).

23 Chapman, D. R., Kuehn, D. M., and Larson, H. K., "Investigation of separated flow in supersonic and subsonic streams with emphasis on transition," NACA Rept. 1356 (1958).

24 Walker, R. E., Stone, A. R., and Shandor, M., "Secondary gas injection in a conical rocket nozzle, I. Effect of orifice diameter and molecular weight of injectant," Appl. Phys. Lab., Johns Hopkins Univ., CM-1010 (February 1962).